A method for surface characterization using solid-state nuclear magnetic resonance spectroscopy demonstrated on nano-crystalline ZnO:Al

Jan Konrad Wied‡[a], Benjamin Mockenhaupt‡[b], Ulrich Schürmann[c], Lorenz Kienle[c], Sebastian Mangelsen[b], Janin Glänzer, Vinicius Ribeiro Celinski[a], Malte Behrens[b]* and Jörn Schmedt auf der Günne*[a]

[a] University of Siegen, Faculty IV: School of Science and Technology, Department for Chemistry and Biology, Inorganic Materials Chemistry and Center of Micro- and Nanochemistry and Engineering (Cμ), Adolf-Reichwein Straße 2, 57076 Siegen, Germany.

[b] Kiel University, Institute of Inorganic Chemistry, Max-Eyth-Straße 2, 24118 Kiel, Germany.

[c] Kiel University, Department of Materials Science, Kaiserstraße 2, 24143 Kiel, Germany.

‡ These authors contributed equally.

* Corresponding authors: E-mail: mbehrens@ac.uni-kiel.de, gunnej@chemie.uni-siegen.de

Abstract

Nano-scale zinc-oxide doped with aluminium ZnO:Al is studied by different techniques targeting surface changes induced by the conditions at which ZnO:Al is used as support material in the catalysis of methanol. While it is well established, that a variety of ^{1}H and ^{27}Al resonances can be found by solid-state NMR for this material, it was not clear yet which signals are related to species located close to the surface of the material and which to species located in the bulk. To this end, a method is suggested which makes use of a paramagnetically impregnated material to suppress NMR signals close to particle surface in the blind-sphere around the paramagnetic metal atoms. It is shown that it is important to use conditions which guarantee a stable reference system relative to which it can be established whether the coating procedure is conserving the original structure or not. This method, called Paramagnetically Assisted Surface Peak Assignment (PASPA), helped to assign the ^{1}H and ^{27}Al NMR peaks to the bulk and the surface layer defined by the blind-sphere of the paramagnetic atoms. The assignment results are further corroborated by the results from heteronuclear $^{27}Al\{^{1}H\}$ dipolar dephasing experiments, which indicate the hydrogen atoms are preferentially located in the surface layer and not in the particle core.

Introduction

The heterogeneous catalyst Cu/ZnO is used for the production of methanol by the hydrogenation of carbon dioxide[1–4] on an industrial scale with a global production of over 85 million tons in the year 2016.[5] The efficient conversion of the greenhouse gas CO_2 to methanol is one of the important current scientific challenges and has triggered an intensive search for improving the catalyst.[6] The activity of the catalyst could be increased significantly by incorporation of a structural promoter, for example Ga^{3+}[7,8], Mg^{2+}[9], and Al^{3+} ions[10,11] into the ZnO support,[12] of which the system ZnO:Al is the subject of this contribution. Al is considered an n-dopant to ZnO and thus should increase the electric conductivity besides.

For a heterogeneous catalyst, materials with high surface area are beneficial. To improve the catalytic activity a detailed understanding of the bulk and surface structure is required including a chemical speciation of different environments of the promoter ions. Different analytical techniques have been used to investigate the incorporation from Al^{3+} into the ZnO support, including infrared spectroscopy[13], RAMAN spectroscopy[14], X-ray diffraction[15], photo-luminescence studies[16], energy dispersed X-ray spectroscopy[17], transmission electron microscopy[18] and high-resolution solid-state NMR spectroscopy (vide infra).

NMR being inherently quantitative and element specific provides information about different types of environments and how they change upon different chemical or thermal treatments of the sample. While the first study by ^{27}Al NMR on ZnO:Al was published in 1997,[19] it is questionable if the study really was conducted on ZnO:Al or rather on a mixture of ZnO and $ZnAl_2O_4$ spinel,[20–22] because of the chosen synthesis conditions. Meanwhile ZnO:Al has been synthesized via different low temperature synthesis routes for example sol-gel synthesis[23], chemical vapour deposition[24], physical vapor deposition[25] or the calcination of hydroxycarbonate precursor materials, which corresponds to the synthesis method of industrial methanol synthesis catalysts.[26] Depending on the synthesis conditions used, different ZnO particle morphologies such as films[27], rods[28] or nanoparticles[29] can be obtained. The first high resolution solid-state ^{27}Al NMR of pure ZnO:Al samples was performed only in the year 2009.[30] By magic-angle-spinning (MAS) four different aluminium environments in ZnO:Al could be resolved in ^{27}Al NMR. The tentative assignment of the signal at δ_{iso}= 82 ppm to a $Al_{Zn}^{\bullet}$ defect in crystalline ZnO could be confirmed by application of quantum chemical calculations and a detailed analysis of

the spectral fingerprint including anisotropic interactions as the chemical shift and the quadrupolar interaction.[31] Because the thermodynamic solubility of Al in ZnO is rather low, it is required to kinetically “trap” the Al inside ZnO by a low temperature synthesis route providing a solubility limit of about 1,3 % aluminium relative to zinc.[32] The other ^{27}Al NMR resonances feature isotropic chemical shift values which indicate, a four-, five- and sixfold coordination, respectively, and their width is consistent with that of disordered or amorphous compounds.[33,34] However it is not clear whether these occur as bulk side-phase, as surface related species or maybe even as a different type of point-defect to ZnO. These ^{27}Al MAS NMR signals can also be observed for Cu/ZnO/Al_2O_3[12,35] and Pd/ZnO/Al_2O_3[36,37] catalysts.

Because Al as an n-dopant should convert ZnO into a metal,[38] it can be expected that the ^{27}Al NMR resonances are subject to a Knight shift, which is related to the conducting electrons and for comparison in metallic aluminium is as big as 1640 ppm.[39] Knight shifted ^{27}Al NMR signals are observed for ZnO:Al synthesized in solution under reflux in a N_2 atmosphere[40,41] and after treatment with a reductive gas atmosphere.[31,42]

Aside from the intended incorporation of foreign ions, ZnO exhibits color center defects[43], oxygen interstitial sites[44,45] and hydrogen defects[46,47] as naturally occurring defects at ambient conditions. Even though hydrogen defects have been evidenced experimentally by IR[48], RAMAN[49], EPR[50] and optical spectroscopy[51] and have been studied by quantum chemical calculations,[52,53] it is not clear if the concentration of these defects is high enough to have any impact on catalytic activity. With respect to solid-state ^{1}H NMR, two different ^{1}H NMR signals, including a fairly sharp signal at ~4.3 ppm, were observed in ZnO and ZnO:Al, which were claimed to correspond to interstitial H positions or the particle surface.[54] It could be shown that these could be removed by annealing at elevated temperatures.[55] What remained unclear in these studies is how humidity and ^{1}H background in NMR probe head could have explained those observations. The strong dominant signals could not be observed for ZnO:Al synthesized from diethylene glycol in a study appearing in the same year.[31] In the latter study evidence from heteronuclear dipolar recoupling experiments showed the H content in the crystalline ZnO:Al phase must be very low, which is inconsistent with the interpretation that a significant amount of H atoms are present on interstitial positions.

In this contribution we pick up an idea introduced by Schilling et al. in the year 2012.[56] In order to identify possible atoms near the particle surface, they treated ZnO:Al with an aqueous manganese(II) acetate solution and recorded spectra before an after treatment.

The expectation was that Mn(II) should act as paramagnetic shift agent and lead to a broadening of the Al resonance in the direct environment. In fact, remarkable changes in the spectrum were observed in peak area and lineshape, which was interpreted by the authors as a confirmation of the previously discussed peak assignments.[31] Even though the solubility of ZnO in water is low with around 1.6 mg/L, not a high amount of water will be required for changing the surface of nano-scale materials. So an open question is to which extent the surface was changed by the treatment especially because the lineshape of the individual ^{27}Al resonances was not conserved. Another question is how Mn(II) would modify the corresponding ^{27}Al NMR spectra. Meanwhile, in the year 2016 in the context of doping-homogeneity-studies, the blind volume/radius around paramagnetic metal atoms has been determined. The blind-sphere is the volume for which the signal is vanishing in the dead-time of the NMR spectrometer and can be determined from NMR visibility curves, i.e. the signal of NMR-active nuclei of the host as a function of the doping concentration.[57–60] Blind-spheres for ^{1}H and ^{31}P in Mn(doped) hopeite $Zn_3(PO_4)_2{\cdot}4H_2O$ of 10 and 7 Å have been reported.[60] These values indicate that the idea presented by Schilling et al.[56] may indeed work and suppress NMR signal from atoms within a surface layer of a few Å.

The purpose of this contribution is to turn **P**aramagnetically **A**ssisted **S**urface **P**eak **A**ssignment (PASPA) into a reliable method to identify signals within the surface layer of nano-scale materials but also to point out problems and potential pitfalls. The possibilities of the method are demonstrated on ZnO:Al obtained by decomposition of a hydrozincite precursor.

Experimental section

Synthesis of the Al-doped $Zn_5(CO_3)_2(OH)_6$ precursor: The co-precipitation of Al-doped hydrozincite $Zn_5(CO_3)_2(OH)_6$ was carried out in an automatically stirred tank reactor (OptiMax, Mettler Toledo) from 1 M metal salt nitrate solutions at a temperature of 65 °C and at a constant pH of 6.5 as described earlier[32]. As precipitating agent, 1.6 M sodium carbonate solution was used. The dosing rate of metal solution with a given Zn:Al-ratio was adjusted to 4.2 g/min and the precipitation agent was dosed on demand in a computer-controlled manner to maintain the pH in the reactor at the desired constant value. After precipitation, the precipitate was aged for 10 minutes without further pH control in the mother liquor. The precursor was washed with deionized water 10 times, to reach a conductivity of the waste water lower than 100 µS/cm and dried at 80 °C over 14 h. The nominal substitution amount of zinc by aluminium is calculated by eqn. 1 and amounts to x_{Al} = 0.03 corresponding to 3% of all Zn cations being substituted by Al:

$$x_{Al} = \frac{n_{Al}}{n_{Al} + n_{Zn}} \quad (1)$$

Synthesis of ZnO:Al: The zinc oxide was synthesized by calcination of grinded hydrozincite from the co-precipitation synthesis. The calcination was performed in static air by heating the compound with a ramp of 2 K/min to a temperature of 320 °C and keeping it there for a duration of 4 h. According to the solubility limit of Al on Zn sites of 1.3%, these conditions have been shown previously to yield different Al species[32] and the sample represents a suitable starting state for species assignment using PASPA. The calcination experiments at higher temperatures were performed under similar conditions by only varying the target temperature. The H_2 treated sample was received by heating the synthesized ZnO:Al to 400 °C for 1 h in a H_2/Ar mixture (7 % H_2). A pure ZnO synthesized the same way but without Al was studied as a benchmark sample for ^{1}H NMR investigations.

Powder X-ray diffraction: X-ray diffraction analysis of the calcined samples was performed on a Bruker D8 advance with Cu-Kα radiation and a LYNXEYE XE-T detector. The diffractograms were recorded in Bragg–Brentano geometry at room temperature between 5° and 90° 2θ. Pawley fits were carried out using TOPAS Academic version 6.0[61] and the instrumental line broadening was described using the fundamental parameter approach[62] as implemented in TOPAS and cross-checked against a measurement of LaB_6 (NIST SRM 660c).

Electron microscopy: The precursors as well as the calcined materials have been investigated by scanning (SEM) and transmission electron microscopy (TEM) to evaluate the particle morphology and size. A spatula tip of the sample was dispersed on a carbon covered stainless steel pin mount sample holder and the SEM micrographs were taken on a Zeiss Gemini Ultra Plus with an Oxford EDX detector. For TEM analysis, a FEI Tecnai F30 G2 STwin (300 kV, FEG) was used. A spatula tip of the ground samples was dispersed in a few drops of n-butanol and prepared on Cu lacey TEM grids.

Impregnation with manganese(II) acetylacetonate: To impregnate a powder of ZnO:Al (x_{Al} = 0.03) with manganese(II) acetylacetonate, $Mn(acac)_2$, saturated solutions with the different solvents (see Fig. 2) were prepared. About 4.2 mmol/L $Mn(acac)_2$ can be dissolved in acetonitrile. Of the saturated solution with the paramagnetic agent a volume of 3 ml was mixed with the ZnO:Al powder (0.1 g). After a time of 30 min the solvent was removed by application of vacuum ($3 \cdot 10^{-2}$ mbar) and simultaneous heating to 60 °C for 14 h. Afterwards, the samples were stored and handled inside an Ar glovebox in order to prevent chemi- and physisorption of water. Solvent blind tests were performed using the pure solvents but otherwise the same conditions.

Nuclear Magnetic Resonance: ^{1}H and ^{27}Al solid-state NMR experiments were performed at 14.1 T on a Bruker Avance Neo NMR spectrometer equipped with a commercial 1.3 mm MAS probe head and a commercial 3.2 mm MAS probe head at a frequency of 600.2 and 156.4 MHz for ^{1}H and ^{27}Al, respectively. The chemical shift values of ^{27}Al are reported on a deshielding scale, relative to a solution of 1.1 M $Al(NO_3)_3$ in D_2O. [63,64] The ^{1}H resonance of 1 % TMS in $CDCl_3$ served as an external secondary reference using the Ξ values for ^{27}Al as reported by IUPAC. The peak areas were determined by deconvolution into mixed Gaussian/Lorentzian profile functions with the program deconv2Dxy relative to central transition ^{27}Al NMR obtained with soft pulses.[65] The ^{27}Al {^{1}H} MAS REDOR NMR experiments were performed at 20 kHz spinning frequency using 23.8 kHz nutation frequency for ^{27}Al. The computation of the REDOR curve was performed using a fortran program (model Fig. S7).[66,67]

Results and Discussion

The target of this contribution is to show how paramagnetic coating can be used to study surface layers of nano-scale materials by NMR. To this end first the PASPA method will be introduced, then it will be shown which requirements need to be met for the application of PASPA. In the next subchapter it will be explained how PASPA results can be interpreted. Thereafter the method is applied to nano-scale ZnO:Al. Finally, the results are discussed and compared to those of other techniques.

Paramagnetically assigned surface peak assignment (PASPA)

PASPA operates on the idea that paramagnetic spin centers suppress the NMR signals from nuclei near the electronic spin. A measure for the suppressed volume is the blind sphere r_{blind}. In principle the suppression ratio can be determined from a measurement of two NMR experiments one with paramagnetic coating and one without, resulting in the peak area A_{para} and A_{ref}, respectively. A reduction of NMR signals from the uncoated compound A_{ref} is interpreted as paramagnetic suppression and thus means that the corresponding signal is caused by an environment close to the particle surface.

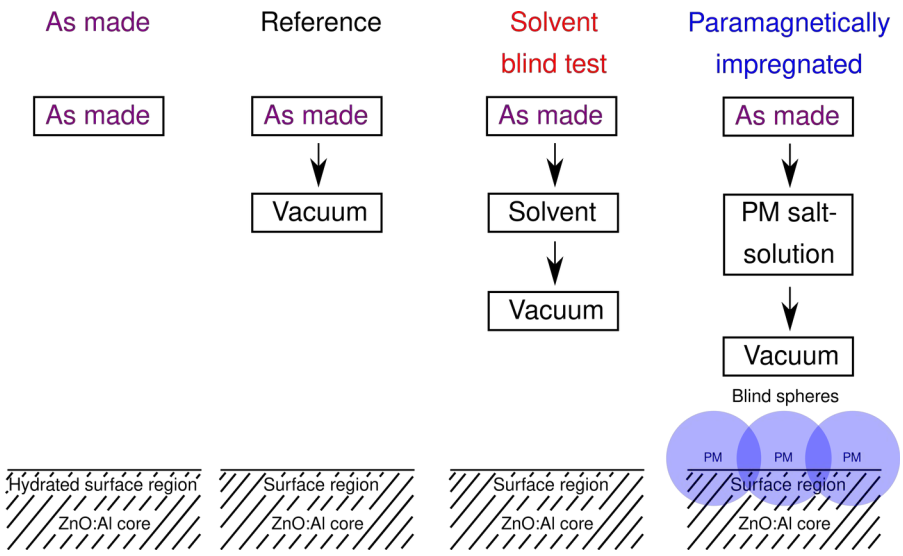

Fig. 1: Schematic representation of the Paramagnetically Assisted Surface Peak Assignment (PASPA) concept, exhibiting the different samples required for a surface assignment of the NMR signals for the example of ZnO:Al. The as made sample is solely treated by vacuum to remove moisture from the surface layer ("Reference"). For the solvent blind test a sample is first treated by the solvent, followed by a vacuum treatment in order to characterize the influence of a solvent on the investigated particle ("Solvent blind test"). Lastly the sample was treated with a paramagnetic metal salt (PM) dissolved in the investigated solvent, followed by a vacuum treatment ("Paramagnetically impregnated"). The blue spheres represent the blind spheres of the paramagnetic metal ion.

The difficulty with the PASPA approach is that paramagnetic coating in principle is a chemical treatment of the *original compound* and measures have to be taken to make sure

that this treatment does not change the object of observation. Chemically we have conducted the *paramagnetic impregnation* by applying a solution of a paramagnetic neutral complex (here $Mn(acac)_2$, acac = acetylacetonate) to the original compound. The solvent is afterwards removed by evaporation at low pressure. To establish a stable reference compound the *reference compound* is defined to be the original compound after treating it in the same way as required for removing the solvent in terms of temperature and pressure (see below). In order to establish whether the solvent treatment has the potential to change the material under investigation it is necessary to perform a *solvent blind test* of a solvent treatment without paramagnetic agent. A suitable solvent system must leave the *reference compound* unchanged, i.e. the NMR spectrum must not change. The advantage of such a protocol (Fig. 1) is that the interpretation of suppression ratio $R_{sup} = (A_{ref}-A_{para})/A_{ref}$ obtained by the PASPA experiment is simple.

Requirements for PASPA

A necessary condition of the PASPA experiment is that the paramagnetic impregnation does not change the original compound. Potentially both the choice of the paramagnetic agent and the solvent required for paramagnetic impregnation can react with the particle surface. To avoid reactions here we have chosen a stable neutral complex, but in principle it could be interesting to even make use of charge to test the preference of surfaces to negatively and positively charged paramagnetic agents. A stable complex like $Mn(acac)_2$ makes it unlikely that REDOX chemistry is taking place. More critical in our opinion is the choice of the solvent. When the idea of paramagnetic impregnation was brought up, Mn^{2+} in water[56] was used. As can be seen from solvent blind test, water does change the ^{27}Al MAS NMR spectrum both in intensities of the peaks and even their lineshape of ZnO:Al which indicates that water is not an "innocent" solvent (Fig. 2). The choice of the solvent clearly depends on the sample under investigation and needs to be tested. For the compound here, ZnO:Al, the solvent acetonitrile appears to be an ideal choice (Fig. 2) as the spectrum of the solvent blind test and the reference compound are almost identical, while water and ethylacetate would produce misleading results.

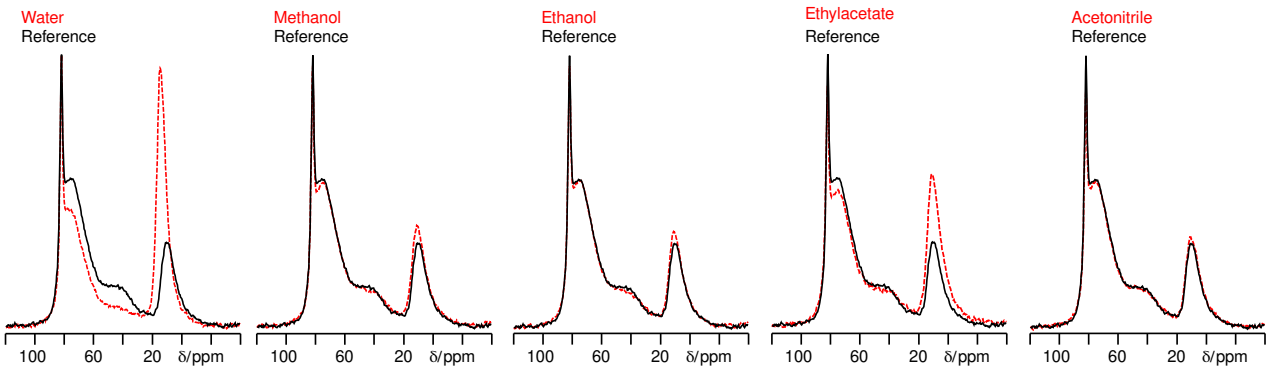

Fig. 2: ^{1}H decoupled ^{27}Al MAS NMR stackplot of ZnO:Al with x_{Al} = 0.03 recorded with 20 kHz rotation frequency, comparing the reference sample (black line) to solvent blind test treated samples (red dotted line). The corresponding solvents used are listed above the spectra.

Interpretation of PASPA results

What can be learned from PASPA experiments? The meaning of a non-zero suppression ratio $R_{sup} = (A_{ref}-A_{para})/A_{ref}$ for a peak is straight forward and indicates that the corresponding atoms are at least partially in the blind sphere of the paramagnetic agent, that is they are located close to the surface of a particle. Species exclusively covering the surface would yield a suppression ratio R_{sup} of 100% if a full coverage of the surface with the paramagnetic agent is achieved. Nevertheless, care should be taken in the interpretation of a low or zero suppression ratio R_{sup}, given that quantitative MAS NMR measured even against internal standards does have errors of a few percent.[68]

Often, from other techniques (see below) the compound morphology of a nano-scale material is known. If it is assumed, that atoms giving rise to a peak are homogeneously distributed through the bulk of a nano-scale material, then it is possible to predict suppression ratios. For spherical particles, the expected suppression ratio R_{sup} is a simple function of the particle radius $r_{particle}$.

$$R_{\mathrm{sup}}^{sphere} \approx 1 - \frac{\left(r_{particle} - r_{blind}\right)^3}{r_{particle}^3} \qquad (2)$$

For needle like structures assuming infinite length and a needle radius r_{needle}, the expected suppression ratio R_{sup} takes a different form.

$$R_{\mathrm{sup}}^{needle} \approx 1 - \frac{\left(r_{needle} - r_{blind}\right)^2}{r_{needle}^2} \qquad (3)$$

For disc like structures assuming infinite disc radius and assuming that both sides are covered by the paramagnetic agent, the expected suppression ratio R_{sup} is a linear function of the disc thickness d_{disc}.

$$R_{\mathrm{sup}}^{disc} \approx 1 - \frac{d_{disc} - 2 \cdot r_{blind}}{d_{disc}} \tag{4}$$

Given the standard -error of the peak area amounts to 3.3% and given the blind sphere amounts to 1 nm, then it can be concluded that PASPA would allow to identify surface-related peaks for spherical nano-particles up to a particle radius of about 28 nm, for needle-like structure up to a needle radius of about 19 nm and for disc-like structures up to a disc thickness of about 20 nm with a three sigma criterion. For bigger structures the relative amount of the surface layer becomes too small to be unambiguously detectable from the normal fluctuation of the NMR signal (see Fig. 3).

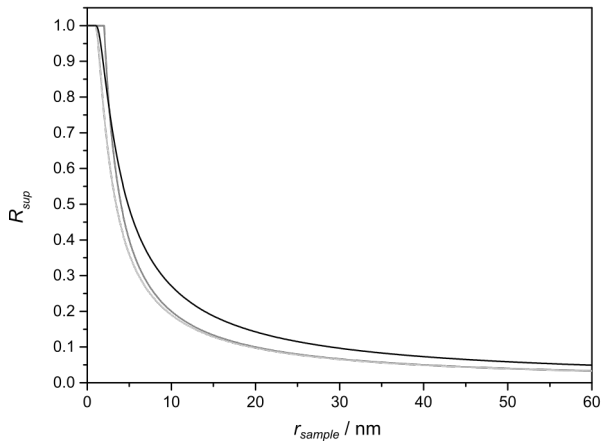

Fig. 3: Plot depicting the effect of the sample size r_{sample} onto the expected suppression ratio R_{sup} of a PASPA experiment for a spherical particle (black line), an infinitely long needle (light gray line) and disc with an infinite radius (gray line) which is paramagnetically impregnated from both sides. A blind sphere of 1 nm is assumed. The NMR detected nucleus is supposed to have a constant number density throughout the particle. For the case of the spherical particle r_{sample} corresponds to particle radius $r_{particle}$, for the needle r_{sample} corresponds to the radius of the needle r_{needle}, and for the case of a disc r_{sample} corresponds to the thickness of the disc d_{disc}. The curves have been computed with the corresponding equations 2-4.

In a similar way, conditions can be derived to investigate if the measured suppression ratio of a specific peak is consistent with the corresponding atoms not being at the surface, meaning that the suppression ratio R_{sup} would be 0 within error limits. What needs further work (not part of this contribution) is to determine the blind-sphere of a paramagnetic agent experimentally in more detail and to reduce the error limits of the quantitative NMR results.

Morphology of ZnO:Al obtained from hydrozincite

For catalysts the surface area and accessibility of it is of high importance. The morphology of the ZnO:Al material presented in this study which was obtained by decomposition of an aluminium doped hydrozincite is well studied by X-ray diffraction and electron microscopy. The precipitation of hydrozincite yields a material which in the scanning electron microscope shows a “broccoli”-like appearance with lobes of a few µm diameter (Fig. 4). The individual lobes consist of intergrown platelets with a thickness of about ~10 nm. So the lobes of the hydrozincite structure mostly consist of free space between solid-platelets, which corresponds to a high surface area and porosity. From this material ZnO:Al is formed by a thermal decomposition process. The product in SEM gives the same “broccoli”-like appearance with lobes of a few µm diameter (Fig. 4) and in SEM it looks like the platelet like structure is conserved besides (Fig. 4). The SEM results thus indicate, that the high surface area of both hydrozincite and of the ZnO:Al formed from it

can be explained by a conservation of the particle morphology, which in a first approximation can be described by platelets of about 10 nm thickness, which indicates that during the process of formation Al atoms can only be transported over short distances of a few nm because otherwise Al would have to be transported through the gas phase which at the low temperatures is unlikely. Heterogeneities on a nm scale of about 10 nm, related to the presence of a minor amount zaccagnite, are thus expected to be a result of the initial precipitation process and not of the thermal decomposition process of hydrozincite.

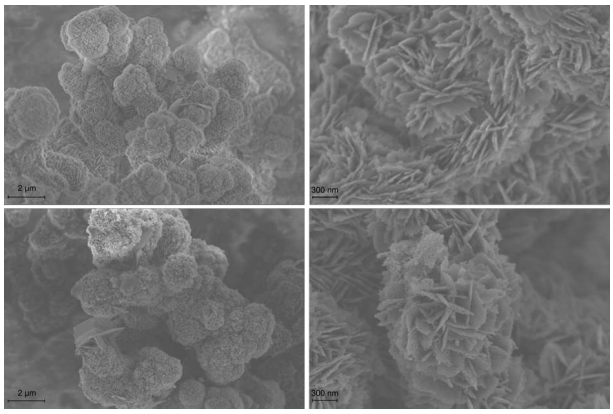

Fig. 4: SEM images of hydrozincite (upper row) and the ZnO:Al (lower row) with x_{Al} = 0.03, exhibiting the platelet-morphology of hydrozincite and ZnO:Al. The larger platelets observed in both materials correspond to zaccagnaite which appears for aluminium concentrations above the kinetic solubility limit of the precursor. [32]

To evaluate, which of the previously mentioned morphologies - spheres, disc/platelets or needles - should be considered for the discussion of the ^{27}Al PASPA NMR experiments, the ZnO:Al materials were further characterized by transmission electron microscopy (TEM) and powder X-ray diffraction (PXRD). TEM images were done ZnO:Al material (Fig. 5). In the scanning TEM (STEM) image (Fig. 5 top) the granular structure of the individual plates is observed, which is in agreement with a model where ZnO particles are growing within the decomposing hydrozincite platelets. The high resolution (HRTEM) micrographs (Fig. 5 bottom) represent the crystal lattice of ZnO:Al particles due to its very low thickness in the range of the 10 nm seen in the SEM. A porosity in the former platelets can be observed also in the range of 10 nm.

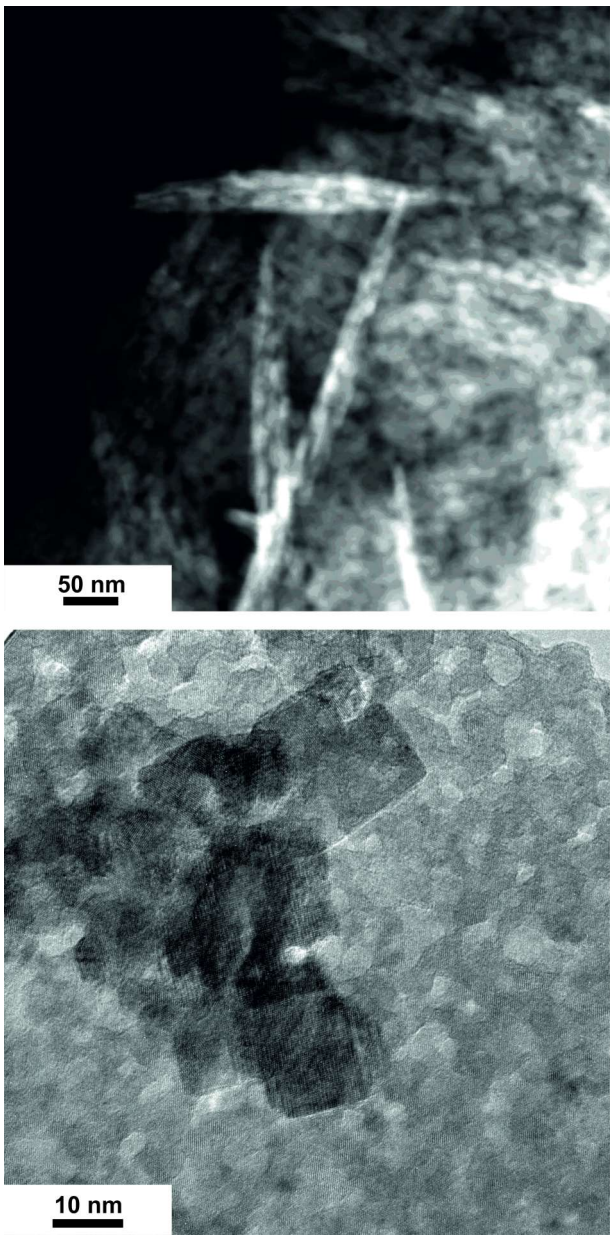

Fig. 5: TEM images of ZnO:Al with x_{Al} = 0.03, showing an overview (top) of several platelets in topview as well as in cross section consisting of small grains of ZnO:Al, and HRTEM micrograph of ZnO:Al crystals (bottom) with x_{Al} = 0.03, showing the crystalline order within these grains.

An analysis of the powder X-ray diffraction pattern results in crystallite sizes of 10.09 ± 0.15 nm for the *h*00 and 15.9 ± 1.5 nm for the 00*l* reflections assuming no significant contribution by defects or strain with a resulting aspect ratio of 1.57. These findings are in accordance to the observation in the TEM.

BET analysis of gas sorption data[32] showed an increase in specific surface area from 14 $m^2\ g^{-1}$ for the hydrozincite material to more than 65 $m^2\ g^{-1}$ for ZnO:Al in agreement with

the development of porosity as observed in SEM and TEM. BHJ analysis resulted in a pore volume of 27 cm^3 g^{-1} and a sharp maximum of the pore size distribution at around 10 nm. This value is close to the estimated size of the primary particles and points to inter-particle pores between these as main contributors to the pore volume, i. e. the pores of these fairly isotropic primary particles should be accessible to impregnation. Their size can be estimated to be 16 nm based on the BET-detected surface area assuming the bulk density of zinc oxide and spherical, non-porous primary particles. The estimated diameter is in reasonable agreement with the results from TEM and with the crystallize size determined by PXRD.

^{27}Al PASPA on ZnO:Al

Given the promising results of Schilling et al.,[56] it was interesting to see if their results could be confirmed with the PASPA scheme and choosing an innocent solvent, i.e. acetonitrile. If the conditions described above are met, rigorous conclusions can be drawn from PASPA experiments based on statistical arguments as demonstrated below. This requires an indirect argumentation by rejecting specific structural models. In the following PASPA will be used to elucidate whether bare ZnO particles are present or particles with a crystalline core and an amorphous shell.

The ^{27}Al MAS NMR spectrum (Fig. 6) exhibits four different aluminium environments present inside the ZnO:Al samples: A well-defined aluminium environment corresponding to the δ_{obs}= 82 ppm ^{27}Al MAS NMR signal, resulting from aluminium on a zinc position in the ZnO crystal lattice $Al_{Zn}^{\bullet}$ and 4-fold (AlO_4), 5-fold (AlO_5) and 6-fold (AlO_6) coordinated aluminium species in disordered/amorphous environments, observed at δ_{obs}= 75 ppm, δ_{obs}= 47 ppm and δ_{obs}= 12 ppm, respectively.

What is interesting, is that the as-made compound and the PASPA reference compound do not have the same lineshape (Fig. 6). The main difference is a vacuum treatment under slightly elevated temperatures which means that a likely explanation is that re-adsorbed water H_2O was evaporated from the compound. If this treatment causes a condensation of hydroxyl functions of Zn-O-H or Al-O-H, then no change in the coordination number of Al would be expected. However, what is observed is a significant decrease of the peak associated to AlO_6 while the peak of AlO_5 increases and the peak of AlO_4 even more. The only explanation for this behavior is that H_2O at least partially acts as a ligand of the Al atoms.

The paramagnetically impregnated sample exhibits a reduction in intensity for the disordered AlO_4, AlO_5 and AlO_6 peaks, while the signal for the $Al_{Zn}^{\bullet}$ defect remains almost unchanged (Fig. S1). This corresponds to suppression ratios R_{sup} of 0.29, 0.47, 0.41 and 0.04 for peaks for the disordered AlO_4, AlO_5 AlO_6 environments and the $Al_{Zn}^{\bullet}$ peak calculated from the peak area per mass ratio of sample ratio, respectively. The error of the suppression ratio 0.056 is estimated from the variation between reference and blind measurement and in good agreement with errors using an external standard for quantification.[68]

Moreover, the success of the paramagnetic impregnation is further observed in a reduction of the T_1 relaxation time of the $Al_{Zn}^{\bullet}$ species from 3.5 s of the reference

compound to 0.88 s for the paramagnetically impregnated sample, i. e. the paramagnetic agent acts as a relaxation enhancer.

For the interpretation of the suppression ratios R_{sup} the results about the particle morphology are required. The suppression ratio for the disordered environments is much lower than what can be explained by statistical errors and thus these signals can clearly be identified as surface related peaks. The suppression ratio R_{sup} of 0.04 for the $Al^{\bullet}_{Zn}$ environment can be compared with the theoretical ratio R_{sup} of spherical particles. The lowest value for the suppression ratio R_{sup} for bare ZnO spherical particles is 18% assuming the biggest estimate for the particle diameter of 16 nm and assuming a reduced blind sphere radius of only 0.5 nm. This conservative guess is more than 2σ away from the experimental value. More likely estimates suggest even higher suppression ratios. Thus, structure models based on bare ZnO particles can be rejected. ^{27}Al PASPA provides strong evidence for a surface layer of the aluminium side phases on the ZnO:Al particles, which explains the hardly measurable signal suppression of the peak for the $Al^{\bullet}_{Zn}$ environment. This conclusion is independent of the presence of a small impurity of zaccagnite in the as-made material which possibly could have consumed a portion of the Al doping. A likely scenario is that a heavily disordered or amorphous layer including the disordered AlO_4, AlO_5, AlO_6 environments covered the ZnO particles.

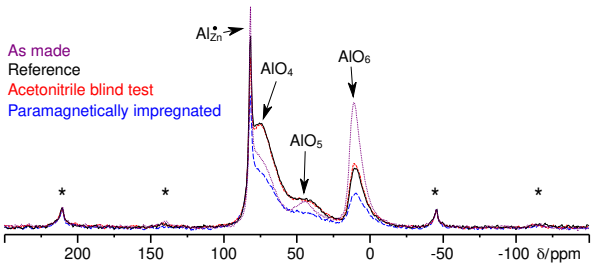

Fig. 6: ^{1}H decoupled ^{27}Al MAS NMR stackplot of ZnO:Al with x_{Al} = 0.03 recorded with 20 kHz rotation frequency, comparing the as-made sample (purple, dotted spectrum) to the reference sample (black, solid spectrum), the acetonitrile blind test sample (red, dashed spectrum) and the paramagnetically impregnated sample (blue, dashed spectrum). The asterisks correspond to spinning sidebands of the $Al^{\bullet}_{Zn}$ resonance. The low suppression ratio R_{sup} for the $Al^{\bullet}_{Zn}$ environment can directly be seen in the good superposition of the peaks of the reference and the paramagnetically impregnated compound in the spinning sidebands.

^{1}H PASPA on ZnO:Al

In the ^{1}H MAS NMR spectra two different signals could be resolved, one sharp at δ_{iso}= 4.3 ppm and a broad signal at around δ_{iso}= 2 ppm (Fig. 7) for the as-made ZnO:Al material. In the vacuum treated reference sample, the sharp ^{1}H MAS NMR peak has vanished. For pure ZnO at various hydration stages similar signals could be observed.[26] These observations are consistent with a peak assignment of the sharp peak at 4.3 ppm to water which has a high degree of mobility on the NMR timescale. The mobility of water molecules for example in a physisorbed state would explain the sharp line-shape lacking MAS spinning sidebands because of the averaging of the ^{1}H-^{1}H dipole-dipole coupling and the removal of dipolar broadening.

Protons from the molecules of this physisorbed water are expected to be in rapid exchange with hydroxyl groups of the type Zn-O-H or Al-O-H, which are assigned to the broad signal at 2 ppm. This effect leads to a small shift of the water peak and reduces the signals of hydroxyl functions. Besides chemisorbed water molecules are expected to act as ligands to six-fold and five-fold coordinated Al atoms, as explained in the discussion of the ^{27}Al MAS NMR spectra. When the surface related water is removed, the protons of the hydroxyl functions, which had been in rapid exchange with mobile water before, can be resolved and give rise to a well distinguishable signal. This mechanism explains the increase of peak area and the change of the line-shape of the OH signal at 2 ppm for the vacuum-treated reference compound (Fig. 7). The loss of mobility is qualitatively in agreement with an increase of the ^{1}H NMR T_1 relaxation times from around 300 ms for the as-made compound to over 600 ms for the reference compound. The observed reduction of the Al coordination number with desorption of H_2O ligands points to the formation of Lewis acidic Al sites at the surface of ZnO:Al by mild thermal activation.[32]

The presented interpretation is further corroborated by the absence of the mobile H_2O signal in a ^{1}H 2D double-quantum single-quantum correlation spectrum, which requires a non-zero ^{1}H-^{1}H dipole-dipole interaction (Fig. S2) for a signal to form, while the broad signal shows strong autocorrelation signals. Moreover, the interpretation is corroborated by ^{27}Al{^{1}H} REDOR experiments, which are in more detail discussed in the next subchapter.

^{1}H PASPA was performed to assign the peaks to the surface and bulk. The ^{1}H NMR signal at 2 ppm features a high suppression ratios R_{sup} of 77%, which means both ^{1}H signals are surface related. This result clearly rules out that ^{1}H atoms mostly occupy interstitial positions in the bulk of the ZnO particles.

What may be irritating, is that the suppression ratio in ^{1}H PASPA for the hydroxyl signal is significantly higher than that for the ^{27}Al peaks from disordered environments observed by ^{27}Al PASPA, even though the signals come from the same “phase” as can be seen from the correlation signals in a ^{27}Al{^{1}H} HETCOR experiment (Fig. S3). This can be explained by the ^{1}H blind-sphere being bigger than that for ^{27}Al, because the blind sphere scales with the cubic root of gyromagnetic ratio of the suppressed nucleus for otherwise identical conditions.[60] Thus the same paramagnetic agent is expected to penetrate deeper into the particle surface in ^{1}H PASPA than in ^{27}Al PASPA. A detailed discussion of the surface structure is presented in the next paragraph.

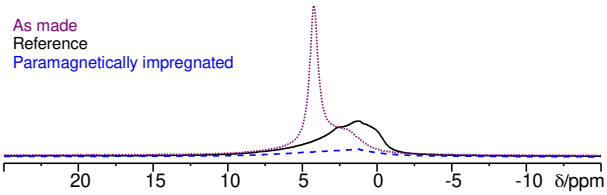

Fig. 7: ^{1}H MAS NMR stackplot of ZnO:Al with x_{Al} = 0.03 recorded with 20 kHz rotation frequency, comparing the as-made sample (purple, dotted spectrum) to the reference sample (black, solid spectrum) and the paramagnetically impregnated sample (blue, dashed spectrum).

A model of nano-scale ZnO:Al from hydrozincite

With the help of ^{1}H and ^{27}Al PASPA, the ZnO:Al particles can be divided into two different regions (Fig. 9). One is the crystalline core of ZnO in which the aluminium species with the $Al_{Zn}^{\bullet}$ environment is present. The other region is the disordered surface layer, to which H_2O, hydroxyl functions, as well as the AlO_6, AlO_5 and AlO_4 environments were assigned. With the help of the ^{1}H PASPA experiment, the H_2O molecules were assigned to the surface, as the corresponding ^{1}H NMR signal is removed by vacuum treatment. This observation was further tested, by annealing a ZnO:Al sample under argon followed by exposure to air (see Fig. S4), which shows that dehydration of the surface is reversible.

A still open question is the presence of H-defects in bulk ZnO as suggested in an earlier paper.[54,55] So far it could be shown that all ^{1}H peaks do have surface relation, but it cannot be rejected that by coincidence a ^{1}H signal with a 2 ppm shift could be found below. A powerful tool to investigate the presence of different types defects in nano-particles is REDOR,[66] because the REDOR effect is dependent on two different kinds of isotopes and their distance, here ^{1}H and ^{27}Al. For the REDOR effect it is possible to describe the influence of thousands of spins efficiently by analytical functions. Because the morphology of the ZnO particles is well studied, it is possible to build a model with an OH surface termination as approximation for the disordered surface layer. A comparison of

experimental and computed $^{27}Al\{^{1}H\}$ REDOR curves can provide information about eventually present H point defects in ZnO and ^{27}Al randomly substituting Zn atoms.

The $^{27}Al\{^{1}H\}$ REDOR curves of the different ^{27}Al signals have been determined for the as-made ZnO:Al material and the vacuum treated materials (Fig. S5, Fig. S6), which qualitatively look similar. The strongest REDOR effect, i.e. quickest rise, can be found for the AlO_6 species, which indicates that the effective dipolar coupling between ^{27}Al and ^{1}H for this peak is the highest, which is in excellent agreement with the claim that the AlO_6 species has a strong affinity to the water molecules. The REDOR effect for the AlO_4 and AlO_5 in disordered environments is clearly present but weaker. The weakest, almost non-existent, REDOR effect can be found for the $Al_{Zn}^{\bullet}$ signal, which directly refutes the presence of H point defects in bulk ZnO. The computed curve as explained above is shown for comparison in Fig. 8. It qualitatively shows a stronger interaction for $Al_{Zn}^{\bullet}$ species positioned inside the ZnO particles with ^{1}H spin at the surface which was generated by terminating the ZnO particle with OH functions. This is evidence for the $AlO_{4/5/6}$ atoms to be part of a surface layer on ZnO, with degrading H concentration which puts an extra distance between the core $Al_{Zn}^{\bullet}$ atoms and the surface related protons. Besides the strength of the REDOR effect, the level to which the dephasing proceeds is relevant. In principle for a pure compound, which contains both ^{1}H and ^{27}Al, the REDOR signal must dephase to 100%. While this is the case for the AlO_6 signal, this is not the case for the AlO_4 and AlO_5 signals of the disordered environments, which indicates that those are at least partially in the hydrogen-depleted interlayer between bulk ZnO and the top surface which hosts the AlO_6 signal.

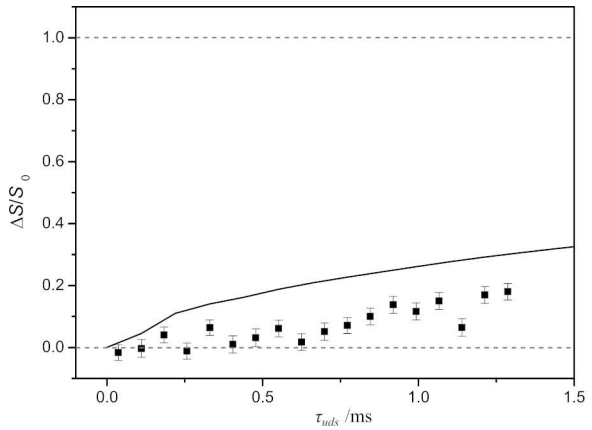

Fig. 8: Computed ^{27}Al {^{1}H} REDOR NMR curve (black line) using the universal dephasing scale[69,70] of the $Al^{\bullet}_{Zn}$ species of a 10x10x14.5 supercell particle, having the particle surface covered by a mono layer hydrogen atoms in form of hydroxyl groups. The computed structure $[Zn_{54900}O_{54899}(OH)_{4561}]^{4559-}$ is shown in the Fig. S7. All positions are assumed to be randomly substituted by ^{27}Al. The Fortran program "Glamor"[67], which was used, implements an analytical formula for the multispin REDOR curve as described in reference [66]. The black dots correspond to the measured ^{27}Al {^{1}H} REDOR NMR curve of the $Al^{\bullet}_{Zn}$ signal in ZnO:Al with x_{Al} = 0.03. The error bars have been derived as described in reference [70].

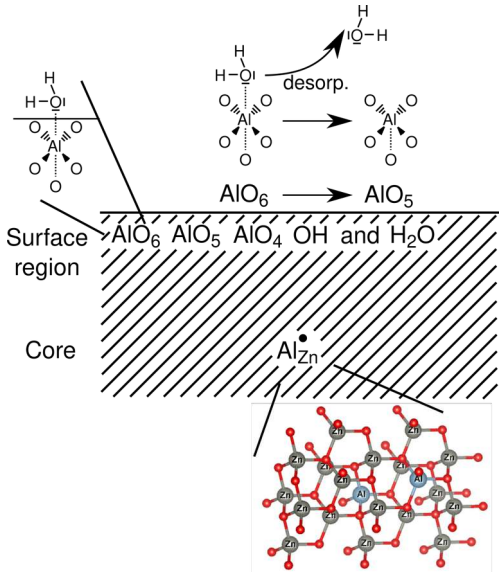

Fig. 9: Schematic representation of a ZnO:Al particle, consisting of 2 regions: the surface layer and the particle core. The particle core consists of crystalline ZnO, where aluminium can be doped on a zinc position. In this region no hydrogen species are present. In the surface layer region the different disordered aluminium species as well as H_2O and hydroxyl groups are located. The upper left structure describes the model for an AlO_6 species, which is coordinated by the lone pair of a H_2O molecule located at the imminent surface. The upper left describes a scheme for the desorption of an AlO_6 coordinating H_2O under the formation of five-fold coordinated aluminium.

Conclusions

In this contribution a method to achieve a chemical speciation of surface related atoms in nano-scale materials is introduced which combines paramagnetic impregnation of nano-scale materials to identify the surface NMR signals. In combination with morphology information from electron microscopy and diffraction this becomes a powerful technique to unambiguously distinguish coated from uncoated nano-particles as demonstrated here on ZnO:Al, for which the presence of Lewis acidic Al sites, which can be activated by dehydration, could be shown.

CRediT author statement

Conceptualization: JSADG and MB; Software: JG, VRC; Formal Analysis: JSADG; Funding Acquisition: JSADG, MB; Investigation: JKW, BM, US, LK, SM, JG, VRC; Project Administration: MB and JSADG, Resources: BM and MB; Supervision: JSADG; Validation: MB and JSADG; Visualization: JKW; Original Draft preparation: JKW, BM, LK, US, SM; Review and Editing: MB, JSADG.

Acknowledgements

We acknowledge financial support by the Deutsche Forschungsgemeinschaft (INST 221/117-1FUGG).

References

[1] S. Kattel, P. J. Ramírez, J. G. Chen, J. A. Rodriguez, P. Liu, *Science (Washington, DC, U. S.)* **2017**, *355*, 1296–1299.
[2] S. Kuld, M. Thorhauge, H. Falsig, C. F. Elkjaer, S. Helveg, I. Chorkendorff, J. Sehested, *Science* **2016**, *352*, 969–974.
[3] M. Behrens, F. Studt, I. Kasatkin, S. Kühl, M. Hävecker, F. Abild-Pedersen, S. Zander, F. Girgsdies, P. Kurr, B.-L. Kniep, M. Tovar, R. W. Fischer, J. K. Nørskov, R. Schlögl, *Science* **2012**, *336*, 893–897.
[4] D. Laudenschleger, H. Ruland, M. Muhler, *Nat. Commun.* **2020**, *11*, 3898.
[5] D. Sheldon, *Johnson Matthey Technol. Rev.* **2017**, *61*, 172–182.
[6] S. G. Jadhav, P. D. Vaidya, B. M. Bhanage, J. B. Joshi, *Chem. Eng. Res. Des.* **2014**, *92*, 2557–2567.
[7] J. Toyir, P. R. De la Piscina, J. L. G. Fierro, N. Homs, *Appl. Catal., B* **2001**, *29*, 207–215.
[8] N. Roberts, R.-P. Wang, A. W. Sleight, W. W. Warren Jr., *Phys. Rev. B: Condens. Matter Mater. Phys.* **1998**, *57*, 5734–5741.
[9] J. Schumann, M. Eichelbaum, T. Lunkenbein, N. Thomas, M. C. Álvarez Galván, R. Schlögl, M. Behrens, *ACS Catal.* **2015**, *5*, 3260–3270.
[10] K. Hagedorn, W. Li, Q. Liang, S. Dilger, M. Noebels, Markus. R. Wagner, J. S. Reparaz, A. Dollinger, J. Schmedt auf der Günne, T. Dekorsy, L. Schmidt-Mende, S. Polarz, *Adv. Funct. Mater.* **2016**, *26*, 3424–3437.
[11] T. Tsubota, M. Ohtaki, K. Eguchi, H. Arai, *J. Mater. Chem.* **1997**, *7*, 85–90.
[12] M. Behrens, S. Zander, P. Kurr, N. Jacobsen, J. Senker, G. Koch, T. Ressler, R. W. Fischer, R. Schlögl, *J. Am. Chem. Soc.* **2013**, *135*, 6061–6068.
[13] H. Serier, M. Gaudon, M. Ménétrier, *Solid State Sci.* **2009**, *11*, 1192–1197.
[14] A. El Manouni, F. J. Manjón, M. Mollar, B. Marí, R. Gómez, M. C. López, J. R. Ramos-Barrado, *Superlattices Microstruct.* **2005**, *39*, 185–192.
[15] M. H. Yoon, S. H. Lee, H. L. Park, H. K. Kim, M. S. Jang, *J. Mater. Sci. Lett.* **2002**, *21*, 1703–1704.
[16] S.-Y. Kuo, W.-C. Chen, F.-I. Lai, C.-P. Cheng, H.-C. Kuo, S.-C. Wang, W.-F. Hsieh, *J. Cryst. Growth* **2006**, *287*, 78–84.
[17] E. M. Seftel, E. Popovici, M. Mertens, K. De Witte, G. Van Tendeloo, P. Cool, E. F. Vansant, *Microporous Mesoporous Mater.* **2008**, *113*, 296–304.
[18] M. Hjiri, L. El Mir, S. G. Leonardi, A. Pistone, L. Mavilia, G. Neri, *Sens. Actuators, B* **2014**, *196*, 413–420.
[19] W. W. Warren Jr., N. Roberts, R. P. Wang, A. W. Sleight, *Mater. Sci. Forum* **1997**, *258–263*, 1365–1370.
[20] M.-Y. Guan, D.-M. Xu, Y.-F. Song, Y. Guo, *Sens. Actuators, B* **2013**, *188*, 1148–1154.
[21] Q. Sun, G. Li, T. Tian, J. Zeng, K. Zhao, L. Zheng, M. Barre, J. Dittmer, F. Gouttenoire, A. Rousseau, A. H. Kassiba, *J. Am. Ceram. Soc.* **2020**, *103*, 3194–3204.
[22] X. Zhao, F. Zhang, S. Xu, D. G. Evans, X. Duan, *Chem. Mater.* **2010**, *22*, 3933–3942.
[23] G. El Damrawi, H. Salaheldin, M. Abdelghany, *Appl. Phys. A: Mater. Sci. Process.* **2021**, *127*, 145.
[24] J.-J. Wu, S.-C. Liu, *Adv. Mater.* **2002**, *14*, 215–218.
[25] H. Rotella, Y. Mazel, S. Brochen, A. Valla, A. Pautrat, C. Licitra, N. Rochat, C. Sabbione, G. Rodriguez, E. Nolot, *J. Phys. D: Appl. Phys.* **2017**, *50*, 485106/1.
[26] M. Wang, G. Yu, W. Ji, L. Li, W. Ding, L. Peng, *Chem. Phys. Lett.* **2015**, *627*, 7–12.
[27] P. Sharma, A. Gupta, K. V. Rao, F. J. Owens, R. Sharma, R. Ahuja, J. M. O. Guillen, B. Johansson, G. A. Gehring, *Nat. Mater.* **2003**, *2*, 673–677.
[28] L. Vayssieres, *Adv. Mater.* **2003**, *15*, 464–466.

[29] T. Xia, M. Kovochich, M. Liong, L. Mädler, B. Gilbert, H. Shi, J. I. Yeh, J. I. Zink, A. E. Nel, *ACS Nano* **2008**, *2*, 2121–2134.
[30] S. Miao, R. N. d'Alnoncourt, T. Reinecke, I. Kasatkin, M. Behrens, R. Schlögl, M. Muhler, *Eur. J. Inorg. Chem.* **2009**, 910–921.
[31] Y. S. Avadhut, J. Weber, E. Hammarberg, C. Feldmann, J. Schmedt auf der Günne, *Phys. Chem. Chem. Phys.* **2012**, *14*, 11610–11625.
[32] B. Mockenhaupt, J. K. Wied, S. Mangelsen, U. Schürmann, L. Kienle, J. Schmedt auf der Günne, M. Behrens, *Dalton Trans.* **2023**, *52*, 5321–5335.
[33] M. Behrens, G. Lolli, N. Muratova, I. Kasatkin, M. Hävecker, R. N. d'Alnoncourt, O. Storcheva, K. Köhler, M. Muhler, R. Schlögl, *Phys. Chem. Chem. Phys.* **2013**, *15*, 1374–1381.
[34] A. Kelchtermans, K. Elen, K. Schellens, B. Conings, H. Damm, H.-G. Boyen, J. D'Haen, P. Adriaensens, A. Hardy, M. K. Van Bael, *RSC Adv.* **2013**, *3*, 15254–15262.
[35] N. Narkhede, H. Zheng, H. Zhang, G. Zhang, Z. Li, *Catal. Sci. Technol.* **2020**, *10*, 7386–7398.
[36] X. Li, C. Zhang, H. Cheng, W. Lin, P. Chang, B. Zhang, Q. Wu, Y. Yu, F. Zhao, *ChemCatChem* **2015**, *7*, 1322–1328.
[37] X. Li, Q. Wu, B. Zhang, C. Zhang, W. Lin, H. Cheng, F. Zhao, *Catal. Today* **2018**, *302*, 210–216.
[38] H. Wang, M. Xu, J. Xu, M. Ren, L. Yang, *J. Mater. Sci.: Mater. Electron.* **2010**, *21*, 589–594.
[39] E. R. Andrew, W. S. Hinshaw, R. S. Tiffen, *J. Magn. Reson.* **1974**, *15*, 191.
[40] R. Noriega, J. Rivnay, L. Goris, D. Kaelblein, H. Klauk, K. Kern, L. M. Thompson, A. C. Palke, J. F. Stebbins, J. R. Jokisaari, G. Kusinski, A. Salleo, *J. Appl. Phys.* **2010**, *107*, 074312/1.
[41] A. Momot, M. N. Amini, G. Reekmans, D. Lamoen, B. Partoens, D. R. Slocombe, K. Elen, P. Adriaensens, A. Hardy, M. K. Van Bael, *Phys. Chem. Chem. Phys.* **2017**, *19*, 27866–27877.
[42] H. Damm, P. Adriaensens, C. De Dobbelaere, B. Capon, K. Elen, J. Drijkoningen, B. Conings, J. V. Manca, J. D'Haen, C. Detavernier, P. C. M. M. Magusin, J. Hadermann, A. Hardy, M. K. Van Bael, *Chem. Mater.* **2014**, *26*, 5839–5851.
[43] V. A. Nikitenko, K. E. Tarkpea, S. F. Nikul'shin, I. P. Kuz'mina, *Zh. Prikl. Spektrosk.* **1987**, *47*, 834.
[44] A. Janotti, C. G. Van de Walle, *Appl. Phys. Lett.* **2005**, *87*, 122102/1.
[45] A. Janotti, C. G. Van de Walle, *Phys. Rev. B: Condens. Matter Mater. Phys.* **2007**, *76*, 165202/1.
[46] E. Ahmed, S. Mazumder, K. Senthilkumar, *Solid State Commun.* **2021**, *339*, 114501.
[47] S. G. Koch, E. V. Lavrov, J. Weber, *Phys. Rev. B: Condens. Matter Mater. Phys.* **2014**, *89*, 235203/1.
[48] E. V. Lavrov, J. Weber, F. Borrnert, C. G. Van de Walle, R. Helbig, *Phys. Rev. B: Condens. Matter Mater. Phys.* **2002**, *66*, 165205/1.
[49] E. V. Lavrov, *Phys. B (Amsterdam, Neth.)* **2009**, *404*, 5075–5079.
[50] N. T. Son, J. Isoya, I. G. Ivanov, T. Ohshima, E. Janzén, *J. Phys.: Condens. Matter* **2013**, *25*, DOI 10.1088/0953-8984/25/33/335804.
[51] E. V. Lavrov, F. Herklotz, J. Weber, *Phys. Rev. B: Condens. Matter Mater. Phys.* **2009**, *79*, 165210/1.
[52] J. Koßmann, C. Hättig, *Phys. Chem. Chem. Phys.* **2012**, *14*, 16392–16399.
[53] F. Bustan Afruz, M. Jafar Tafreshi, M. R. Mohammadizadeh, M. Fazli, *Comput. Mater. Sci.* **2018**, *143*, 232–239.

[54] J. K. Park, K. W. Lee, W. Lee, C. E. Lee, D.-J. Kim, W. Park, *Solid State Commun.* **2012**, *152*, 116–118.
[55] J. K. Park, K. W. Lee, C. E. Lee, *Solid State Commun.* **2013**, *165*, 19–21.
[56] C. Schilling, M. Zähres, C. Mayer, M. Winterer, *J. Nanopart. Res.* **2014**, *16*, 1–15.
[57] W. Li, M. Adlung, Q. Zhang, C. Wickleder, J. Schmedt auf der Günne, *ChemPhysChem* **2019**, *20*, 3245–3250.
[58] W. Li, V. R. Celinski, J. Weber, N. Kunkel, H. Kohlmann, J. Schmedt auf der Günne, *Phys. Chem. Chem. Phys.* **2016**, *18*, 9752–9757.
[59] W. Li, P. F. Smet, L. I. D. J. Martin, C. Pritzel, J. Schmedt auf der Günne, *Phys. Chem. Chem. Phys.* **2020**, *22*, 818–825.
[60] W. Li, Q. Zhang, J. J. Joos, P. F. Smet, J. Schmedt auf der Günne, *Phys. Chem. Chem. Phys.* **2019**, *21*, 10185–10194.
[61] A. A. Coelho, *J. Appl. Crystallogr.* **2018**, *51*, 210–218.
[62] R. W. Cheary, A. A. Coelho, J. P. Cline, *J Res Natl Inst Stand Technol* **2004**, *109*, 1–25.
[63] R. K. Harris, E. D. Becker, *J. Magn. Reson.* **2002**, *156*, 323–326.
[64] R. K. Harris, E. D. Becker, S. M. Cabral De Menezes, P. Granger, R. E. Hoffman, K. W. Zilm, *Pure Appl. Chem.* **2008**, *80*, 59–84.
[65] D. Jardón-Álvarez, J. Schmedt auf der Günne, *Solid State Nucl. Magn. Reson.* **2018**, *94*, 26–30.
[66] V. R. Celinski, J. Weber, J. Schmedt auf der Günne, *Solid State Nucl. Magn. Reson.* **2013**, *49–50*, 12–22.
[67] J. Glänzer, V. R. Celinski, J. Weber, J. Schmedt auf der Günne, *https://github.com/storkan/Glamor* **2024**.
[68] Y. S. Avadhut, D. Schneider, J. Schmedt auf der Günne, *J. Magn. Reson.* **2009**, *201*, 1–6.
[69] T. Gullion, J. Schaefer, *J. Magn. Reson.* **1989**, *81*, 196–200.
[70] M. Roming, C. Feldmann, Y. S. Avadhut, J. Schmedt auf der Günne, *Chem. Mater.* **2008**, *20*, 5787–5795.